Available online at www.sciencedirect.com
ScienceDirect
Biochimica et Biophysica Acta 1758 (2006) 892–899
BIOCHIMICA ET BIOPHYSICA ACTA
BBA
www.elsevier.com/locate/bbamem

Review

Brain tissue characterisation by infrared imaging in a rat glioma model

Nadia Amharref [a], Abdelilah Beljebbar [a,*], Sylvain Dukic [a], Lydie Venteo [b], Laurence Schneider [b], Michel Pluot [b], Richard Vistelle [a], Michel Manfait [a]

[a] *Unité MéDIAN, CNRS-UMR 6142, UFR de Pharmacie, IFR 53, Université de Reims Champagne-Ardenne, 51 rue Cognacq-Jay, 51096 Reims cedex, France*
[b] *Laboratoire Central d'Anatomie et de Cytologie Pathologiques, CHU Robert Debré, Avenue du Général Koenig, 51092 Reims cedex, France*

Received 6 January 2006; received in revised form 12 April 2006; accepted 1 May 2006
Available online 16 May 2006

Abstract

Pathological changes associated with the development of brain tumor were investigated by Fourier transform infrared microspectroscopy (FT-IRM) with high spatial resolution. Using multivariate statistical analysis and imaging, all normal brain structures were discriminated from tumor and surrounding tumor tissues. These structural changes were mainly related to qualitative and quantitative changes in lipids (tumors contain little fat) and were correlated to the degree of myelination, an important factor in several neurodegenerative disorders. Lipid concentration and composition may thus be used as spectroscopic markers to discriminate between healthy and tumor tissues. Additionally, we have identified one peculiar structure all around the tumor. This structure could be attributed to infiltrative events, such as peritumoral oedema observed during tumor development. Our results highlight the ability of FT-IRM to identify the molecular origin that gave rise to the specific changes between healthy and diseased states. Comparison between pseudo-FT-IRM maps and histological examinations (Luxol fast blue, Luxol fast blue-cresyl violet staining) showed the complementarities of both techniques for early detection of tissue abnormalities.

Keywords: Brain tumor; Glioma; Peritumoral infiltration; FT-IR microspectroscopy; Multivariate statistical analysis; Early diagnosis

Contents

1. Introduction . . . 893
2. Materials and methods . . . 893
 2.1. Animal model . . . 893
 2.2. Glioma cell lines . . . 893
 2.3. Intracerebral inoculation . . . 893
 2.4. Sample preparation . . . 893
 2.5. Staining of myelinated fibers with Luxol Fast Blue . . . 893
 2.6. Counterstaining with cresyl violet . . . 893
 2.7. FT-IRM spectra . . . 893
 2.8. Data pre-treatment . . . 893
 2.9. Data treatment . . . 894
3. Results . . . 894
4. Discussion . . . 896
Acknowledgements . . . 898
References . . . 898

Abbreviations: FT-IRM, Fourier transform infrared microspectroscopy; H&E, Hematoxylin and eosin; LFB, Luxol fast blue; LFB-CV, LFB counterstained with cresyl violet; ZnSe, Zinc Selenide; MCT, Mercury–cadmium–telluride; SNV, Standard normal variate; PCA, Principal component analysis; KM, K-means

* Corresponding author. Tel.: +33 3 2691 8376; fax: +33 3 2691 3550.
E-mail address: abdelilah.beljebbar@univ-reims.fr (A. Beljebbar).

0005-2736/$ - see front matter © 2006 Elsevier B.V. All rights reserved.
doi:10.1016/j.bbamem.2006.05.003

1. Introduction

Malignant cerebral tumors account for 1 to 2% of all cancers, and among those, 30% are gliomas [1]. Gliomas are tumors which infiltrate the cerebral parenchyma gradually, increasing intracranial pressure and causing neuronal loss. In spite of a growing therapeutic arsenal, treatment of glioblastomas remains difficult, and median patient survival has not changed over the last 20 years. In addition to surgery and radiotherapy, chemotherapy protocols are often set up, allowing, in certain cases, an increase in the lifespan of patients [2]. This result, although modest, justifies the continuation of the investigations aiming at the development of new powerful techniques to better understand the molecular pathogenesis of glioma. As such, better knowledge of the dynamics of tumor invasion and neovascularisation appears to be crucial for the development of new therapeutic approaches.

Fourier transform infrared microspectroscopy (FT-IRM) is a technique sensitive to molecular composition and molecular conformational changes associated to tumor development not easily detectable by morphological methods. Previous studies have demonstrated the potential of this technique in discriminating diseased from healthy tissue [3,4], apoptotic and necrotic tissues [5,6], sensitive and multi-resistant cells [7], and the effect of anti-cancer chemotherapy [8,9].

In this study, FT-IRM was used to investigate the molecular changes associated with the development of brain glioma. Multivariate statistical analysis and imaging was applied to discriminate normal brain structures from tumor and surrounding tumor tissues. The experimental C6 Rat glioma model was chosen because of its similar morphology to glioblastoma multiform and its rapid proliferation rate. Data obtained with FT-IRM, were correlated with histopathological examinations to understand the molecular changes associated with tissue alteration.

2. Materials and methods

2.1. Animal model

Male Wistar rats, weighing between 260 and 300 g, (Elevage Dépré, France) were individually housed in a controlled environment (20±2 °C; 65±15% relative humidity) and maintained under a 12:12 h light:dark cycle. They had access to food (U.A.R., France) and tap water ad libitum. They were randomly allocated to one of two study groups: Control and C6 tumor. All animal procedures adhered to the "Principles of laboratory animal care" (NIH publication #85-23, revised 1985) and the European Community guidelines for the use of experimental animals.

2.2. Glioma cell lines

The C6 glioma cell line was initially produced by means of weekly injections of N-methylnitrosourea [10]. C6 cells were maintained in NUT.MIX.F-12 (HAM) minimum essential medium containing 10% fetal calf serum (GibcoBRL, France). They were grown to confluence in a humidified atmosphere of 5% CO_2 at 37 °C. Exponential growth cultures were harvested with a solution of 0.05% trypsin and 0.02% EDTA, and resuspended in NUT.MIX.F-12 (HAM) medium. Cells were washed three times in NUT.MIX.F-12 (HAM) medium and viable cells counted by a trypan blue dye exclusion method. Finally, cells were suspended in NUT.MIX.F-12 (HAM) minimum essential medium to a final concentration of 5.10^6 cells per 10 µl for intracerebral inoculation.

2.3. Intracerebral inoculation

Rats were anesthetised by i.p. injection of 10 mg/kg xylazine (Bayer, Germany) and 100 mg/kg ketamine (Parke-Davis, France). Their head was mounted into a stereotactic head holder (Stoelting model 51600, Phymep, France) in a flat-skull position, the scalp cleaned with 70% ethanol, and the skull exposed by a midline incision. A small burr hole was drilled into the right side at a location defined by the following stereotactic coordinates: 1 mm anterior to the bregma; 3 mm lateral from the midline. Ten microliters of the tumor cell suspension were then injected with a syringe over 2 min at a depth of 4 mm from the skull surface, coordinates corresponding to the caudate putamen (CP).

2.4. Sample preparation

Twenty days after tumor cell injection, control and tumor bearing rats were sacrificed and their brains removed. Macroscopic sections (2 mm) wide were immediately performed and frozen in methyl-butane cooled with liquid nitrogen. For each section, 8 µm thick samples were sectioned with a cryostat and placed on Zinc Selenide (ZnSe) transparent infrared windows. Three adjacent tissue sections were routinely stained with hematoxylin and eosin (H&E), Luxol fast blue (LFB), and LFB counterstained with cresyl violet (LFB-CV) for microscopic examination. The histopathological H&E staining was used to determine the zone of interest for FT-IRM measurement.

2.5. Staining of myelinated fibers with Luxol Fast Blue

Briefly, slide-mounted 8 µm cryosections were fixed in formaldehyde for 1 h, rinsed in distilled water, and transferred through 95% ethanol to a 0.1% solution of LFB (MBS, Sigma, France) in 95% ethanol and 0.05% acetic acid. After staining overnight at 58 °C, sections were washed with distilled water, and subsequently with PBS, differentiated in 0.05% aqueous lithium carbonate followed by 70% ethanol, and washed in distilled water before standard mounting, dehydrating, and cover slipping.

2.6. Counterstaining with cresyl violet

Slide-mounted sections were rinsed with distilled water and incubated for 10 min in a solution of cresyl violet (Sigma, France) in acetate buffer, dehydrated through a graded series of ethanol, and coverslipped. A color video camera (DC300, Canon, France) attached to a microscope (DMRB, Leica, Germany) captured histological sections as digital images that were further enhanced on a computer using IM50 (version 1.20, France).

2.7. FT-IRM spectra

FT-IRM spectra were recorded on a Spectrum Spotlight 300 infrared imaging spectrometer (Perkin-Elmer instrument, UK) coupled to an IR microscope with a liquid nitrogen cooled 16×1 Mercury–Cadmium–Telluride (MCT) array detector. The array detection mode allows the generation of molecular specific images over a total area of 1.64 cm^2. Pixel resolution used in this study was 25 µm, thus allowing images to be collected more rapidly than the serial collection point detector. The array detector provides a useful spectral range of 720 to 4000 cm^{-1}. The microscope was equipped with a movable, software controlled, x,y stage directly linked to the spectrometer's interferometer and synchronised to move every time the interferometer changed direction up to five times per second. The stage position was highly reproducible (CV: 0.001%) and much easier to control than the moving mirror position in a step scan spectrometer. Spectra were recorded with a final resolution of 4 cm^{-1}, with two accumulations for each point. Data acquisition was carried out by means of the Spotlight software package (V. 1.1.0, PerkinElmer, Paris).

2.8. Data pre-treatment

To allow meaningful comparisons, all FT-IRM data were uniformly pretreated. After atmospheric correction, all spectra (in the regions 900–1800 cm^{-1}) were converted to their first derivative using a seven point

Savitzky–Golay algorithm to minimise the influence of background artifacts. The resulting spectra were then scaled using a Standard Normal Variate (SNV) procedure [11]. In this transformation, every spectrum is mean centered (so that the average of the spectral intensities in all wavenumber channels is zero) and scaled to have a standard deviation of one.

2.9. Data treatment

After appropriate pre-treatment, a multivariate statistical analysis was performed to extract the desired clinically relevant data from FT-IRM spectra. Data from healthy and cancer brain tissues were placed in a similar matrix and processed by Principal Component Analysis (PCA) and K-Means (KM) clustering analysis to build maps with similar color scales. The aim of this data processing was to find common and discriminating structures between healthy and tumor tissues by comparing their infrared maps.

PCA was performed on the data to remove redundancies at different locations in the spectra by finding the independent sources of variation in all spectra, and to reduce the number of variables describing the data set. Maps based on principal component scores were then used to find the independent sources associated with healthy and cancer brain tissues. K-means clustering was performed on these principal component scores instead of on raw data to handle the large amount of data obtained during FT-IRM mapping experiments. KM clustering is a non-hierarchical clustering method, which gives a ''hard'' (crisp) class membership for each spectrum, (i.e., the class membership of an individual spectrum can only take the values 0 or 1) [12–14]. In the present study, we used a setting of 100 for the maximal number of iterations and up to 10 for the number of clusters.

Pseudo-color maps based on cluster analysis were then created by assigning a color to each spectral cluster. Each spectrum of a mapping experiment had a unique spatial x,y position in the map, and false-color images could be generated by specifically plotting colored pixels as a function of their spatial coordinates. Spectra of different clusters ideally exhibit different spectral signatures. The cluster components were calculated by averaging the clusters and used for the interpretation of the chemical or biochemical differences between clusters [15].

The processing analysis on FT-IRM data was performed with Matlab (Version 5.3, MathWorks, Inc., Matick, USA).

3. Results

Multivariate statistical analysis was performed on a data set containing all FT-IRM measurements obtained from healthy and tumor brain tissues. Seven clusters describing both healthy and cancer features, and one cluster corresponding to ZnSe, were extracted and the pseudo FT-IRM maps were constructed with the same color scale.

Fig. 1C displays an infrared map obtained from healthy brain tissue. In this pseudo-color map, 5 clusters were sufficient for describing all normal brain features. FT-IRM images allow clear identification of the anatomical structures of the rat brain. Gray matter (e.g., cortical cortex), which naturally has a much higher content of water and proteins, was encoded by four colors (yellow, red, brown and cyan). Grey cluster in the image seems to correlate with white matter tissue, the corpus callosum (CC), and commissura anterior (CA). Cyan-colored areas are typical for one structure of cortex and around the caudate putamen (CP) which are heavily myelinated and consist largely of lipids. However, other colors, associated with cortex, seem to correspond to the differing lipid content.

An infrared spectrum of brain tissue is a fingerprint that reflects its composition. To illustrate this molecular specificity for brain features, Fig. 2 shows class average of the normal tissue class. These spectra are dominated by two absorbance bands at 1656 and 1546 cm^{-1} known as the amide I and II, respectively. Amide I arises from C═O hydrogen bonded stretching vibrations and amide II from C–N stretching and CNH bending vibrations. The weaker amino acid side chain from peptides and proteins at 1452 cm^{-1} was associated with the asymmetric and symmetric CH_3 bending vibrations. The band at 1740 cm^{-1} arises from the stretching mode of C═O groups of lipids. The strongest bands, at 1236 cm^{-1} and 1084 cm^{-1} are due to the asymmetric and symmetric phosphate stretching mode PO_2^-, respectively. The relatively weak band at 1172 cm^{-1}, in the healthy tissue is due to stretching mode of C–O groups of proteins [7]. The bands located at 1466 cm^{-1} and 1382 cm^{-1} are due to CH_2 and CH_3 banding of cholesterol and/or phospholipids [16] strongly representing in component 8 which is characteristic of CC. Moreover, all normal brain structures were characterised by a variation in the peak position and intensities of all these previous bands. In fact, lipids content decreased around CC and disappeared in the cortex.

Comparison between pseudo-color maps and the histopathology images (Fig. 1A) shows that the FT-IRM image provides more information on the cortex and around CP than standard histopathology. In fact, four layers were identified from the cortex, whereas, H&E staining did not allowed to discriminate between the layers in the cortex. LFB staining was then used to visualise myelin distribution into brain tissues and to map particular sections within the cortex. In stained preparations, myelin is intensely blue, so that white matter is well differentiated from gray matter (Fig. 3A). In fact, large fiber tracts like CC, CA and some bundles in CP can be easily recognised. In Fig. 3A, LFB staining shows a gradation color density between brain structures. CC and CA present an important lipid content due to high myelin level in these structures involved in communication within and between hemispheres. However, even with higher magnification it was very difficult to distinguish between all cortex layers because this staining is mainly restricted to fibers. Thus, the individual cell type cannot be recognised within the tissue. This LFB staining was then combined with cresyl violet coloration to stain not only rough endoplasmic reticulum (Nissl substance) but chromatin and nucleoli as well. This coloration was used in our study to visualise all the different cell types present in the cortex (Fig. 3B). With this coloration six different layers were then identified in the cortex instead of four layers in the FT-IRM map. On the other hand, when multivariate statistical analysis was applied only on FT-IRM data measured from normal brain tissue we were able to distinguish between five cortex layers. This pseudo-color map was correlated with that obtained with LFB-CV staining (Fig. 3B). The outermost molecular layer (I) containing non-specific fibers, corresponds to the yellow cluster. The external granular layer (II) is a rather dense layer composed of small cells. The external pyramidal layer (III) contains pyramidal cells, frequently in row formation. The internal granular layer (IV) is usually a thin layer with cells similar to those in the external granular layer. These layers II, III and IV were not clearly discriminated and seem to correspond to the red and blue clusters. The ganglionic layer (V) contains, in most areas,

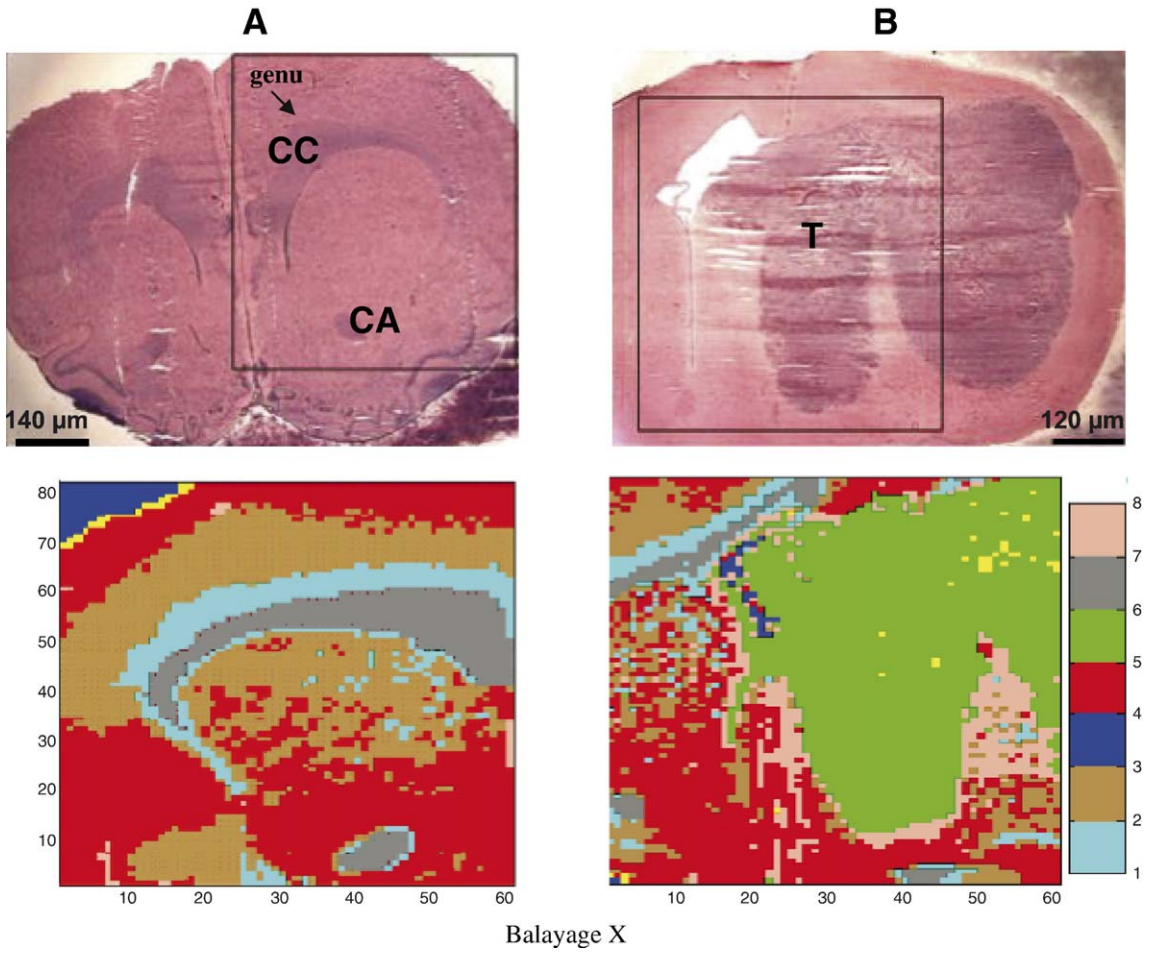

Fig. 1. Photomicrography of HE stained healthy brain tissue (A) and glioma tissue (B) sections. In figure (A), particular structures can be recognised such as CC that appears as a "V" shape with the genu (apex) pointing medially, and CA. In figure B, the more intensely stained area, marked "T" represents tumor zone. The pseudo-color FTIR maps (C) and (D) were obtained from the measured areas marked with a black frame on the adjacent unstained healthy (A) and glioma (B) tissues, respectively. The size of the measured area was 5.5×7.6 mm^2 for both tissues. 60×80 spectra (expressed in pixels) were recorded on these areas of interest. Pseudo-color FTIR maps were constructed on 8-means clusters. Each cluster (consisting of similar spectra) was assigned to one brain feature. Blue: denotes areas in the scan where no tissue was present; yellow, red, brown and cyan: Cortex areas; grey: CC and CA areas; green: tumor tissue area; pink: infiltrative zone.

pyramidal cells that were fewer in number but larger in size than those in the external pyramidal layer (brown). The fusiform layer (VI) consists of irregular fusiform cells whose axons enter the adjacent white matter known as the CC (cyan) [17].

Since tissue composition is altered by tumor invasion, infrared spectra of malignant glioma differ from that of normal tissue. We have investigated the molecular changes associated with malignant rat brain tumor. Fig. 1D displays an infrared map obtained from tumor brain tissue and constructed on 7/8 clusters. This pseudo-color map shows some common structures with normal tissue such as CC, and three layers associated with cortex (cyan, red and brown). Other structures were restricted to tumor tissue (component 6 and 8). The component 8 was located around the tumor and could be attributed to the oedema. Indeed, brain tumors contain tumor vessels that may have different structural properties favouring the formation of oedema within and around the tumor. Ide et al. found a correlation between peritumoral brain oedema and cortical destruction by the tumor [18]. Fig. 1D shows also the recoil of CC by tumor development. The difference spectrum between normal and tumor structures were prominent by lipid features meaning that the contribution of fat in the tumor tissue decreased. Our data showed molecular changes between healthy and tumor tissue (Fig. 2A). In fact, the relatively weak band at 1172 cm^{-1}, in the healthy tissue, due to stretching mode of C–O groups of proteins, decreased and shifted to 1190 cm^{-1} in the tumor and surrounding tumor spectra. The weaker amino acid side chain from peptides and proteins at 1452 and 1392 cm^{-1} are associated with the asymmetric and symmetric CH_3 bending vibrations. In the malignant brain, i) the lipid/proteins ratio (1466/1452 cm^{-1}) decreased, ii) the band at 1740 cm^{-1} become weak and even disappeared when compared to the corresponding bands in healthy. The variations of the spectral characteristics of the FT-IRM spectra between the normal and malignant tissues provided a basis for clinical application.

The study of the frequency region 1000–1350 cm^{-1} revealed significant differences in the infrared spectra between healthy and tumor tissues. The bands at 1070 cm^{-1} and 1084 cm^{-1} are

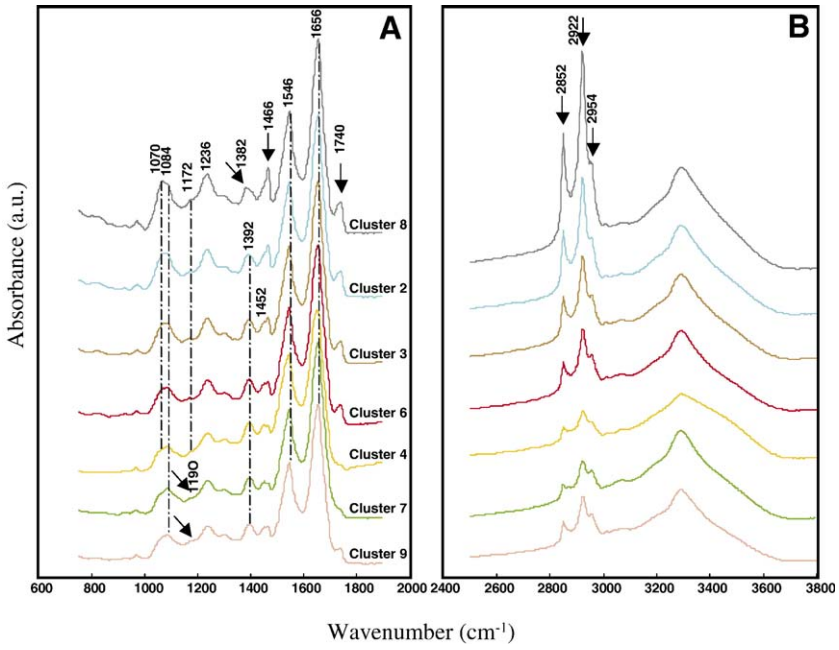

Fig. 2. Representative cluster-averaged IR spectra collected from healthy brain and glioma tissue sections in the spectral region (A) 750 cm^{-1} to 1900 cm^{-1}, and (B) 2500 cm^{-1} to 3800 cm^{-1}. Spectra are shown with the same color scale than in pseudo color maps C and D.

due to the C–C stretching and symmetric phosphate stretching mode PO_2^-, respectively. In all case, when compared with healthy tissues, the malignant tissues displayed a decreased intensity of the asymmetric PO_2^- (1236 cm^{-1}) band and of the C–C stretching (1070 cm^{-1}) band, an increased intensity of the symmetric PO_2^- (1084 cm^{-1}) band, and changes in the shape of these bands (become large).

The lipids spectra contain a large proportion of methyl, methylene and carbonyl bands in the region 2600–3700 cm^{-1}. Fig. 2B displays the infrared spectra of healthy and malignant glioma tissues in this region. The bands at 2852 cm^{-1} and 2922 cm^{-1} were due to the symmetric CH_2 stretching mode of the membrane lipid. The band at 2954 cm^{-1} is due to asymmetric CH_3 stretching mode of the methyl group. The asymmetric CH_3 stretching of lipids and proteins contribute to the intensity of the band at 2954 cm^{-1}. The bands were assigned to CH_2, CH_3 stretching vibrations of cholesterol and phospholipids. In the malignant tissues, the intensity of the CH_2 band CH_3 bands decreased compared to the corresponding bands in healthy tissue.

LFB and LFB-CV staining were used to visualise myelin distribution into tumor brain tissues (data not shown). Some normal features such as CC, CA, and CP were recognised but these colorations failed to reveal the tumoral and peritumoral part of the tissue.

4. Discussion

The objective of this study was to determine tissue modifications between tumoral and healthy brain tissue and to better identify the nature of the surrounding tumor tissue by FT-IRM. FT-IRM images presented here allow clear identification of anatomical structures of the healthy rat brain (CC, CA, and cortex), changes associated to tumor and the surrounding tumor. Our results demonstrate the potential of this technique in successfully discriminating between healthy, tumoral, and surrounding tumor tissues.

In fact, the grey structure in the image seems to correlate with white matter tissue (e.g., which is more myelinated and consist largely of lipids, i.e., fats). The other colors seem to correspond to the differing contents of fat in brain tissue. The gray matter of the brain (e.g., Cortex, CP), which naturally has a much higher content of water and proteins, was described with 3 components with different lipid content. This fat distribution in brain tissue was correlated to the degree of myelination.

As the image contrast is based on the vibrational signature of the tissue components, FT-IRM imaging does not require the use of dyes, tags or stains. On the other hand, histopathological diagnosis depends on visualisation of the sample morphology by staining technique. In spectral diagnosis, objective intrinsic structural and morphological information, on measured area, were simultaneously collected. By correlating FT-IRM spectral maps with histopathology (H&E, LFB, and LFB-CV) of the adjacent tissue sections, we highlighted the potential of FT-IRM to identify the morphologic origin that gave rise to the specific spectral features found in this study. In fact, with standard staining (H&E), we were not able to discriminate between the different cortex layers. On the other hand, FT-IRM pseudo-color maps were clearly similar to LFB-CV staining for visualising myelin distribution in healthy brain tissues (white and gray matters). Yet, this staining technique failed to visualise the tumor and peritumoral part of the tissue.

This spectroscopic study pointed out different cortex layers which are not easily detectable by morphological methods alone. The cortex consists of a thin layer of gray substance which covers the two hemispheres and whose thickness varies

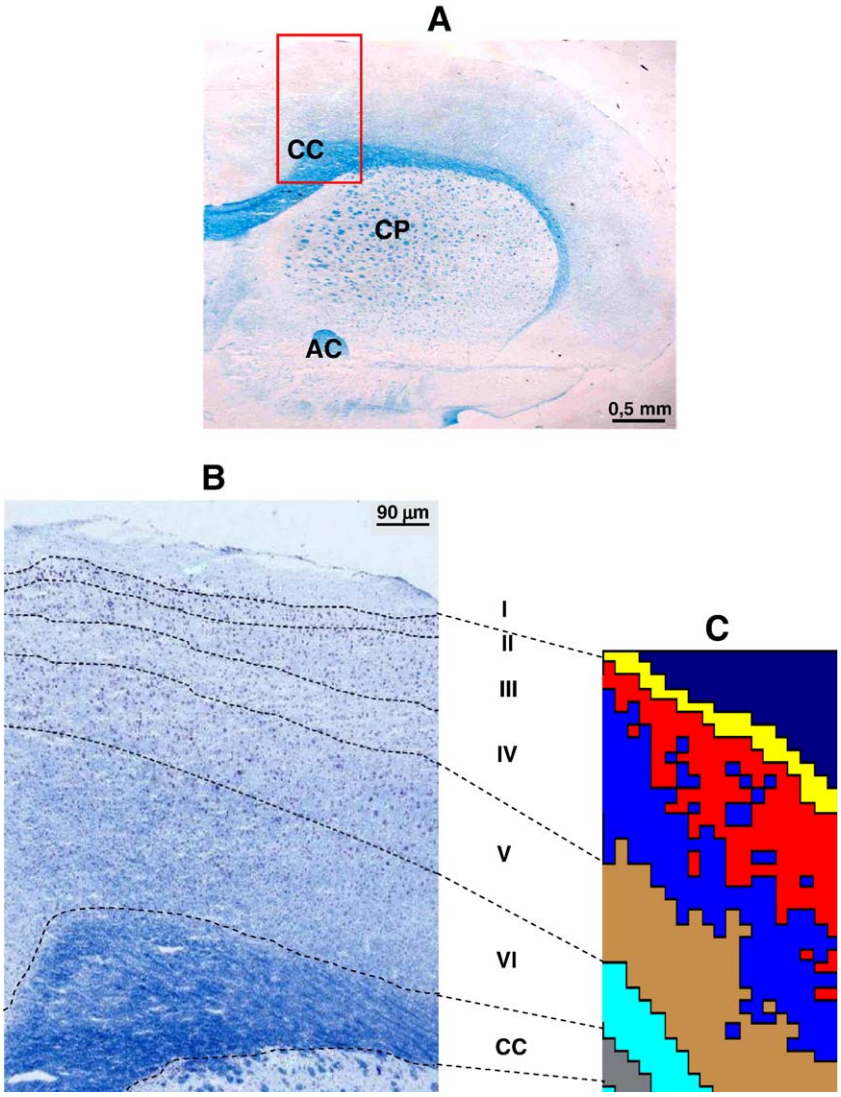

Fig. 3. Photomicrography of a brain tissue section at low (A) and high (B) magnification, respectively. (A) is stained with LFB; in this image CC, CA and CP appears more lightly stained. (B), a small area of (A) marked with a red frame, stained with LFB-CV, pointing out the cortical layers of the rat cortex. Pseudo-color FTIR map (C) based on K-means cluster analysis applied only on FTIR data measured from normal brain tissue. The complementarity between structural (C) and morphological (B) information is represented by a dotted line. Yellow: Layer I of the cortex. Red and blue: Layers II, III and IV; brown: Layer V, cyan: Layer VI and grey: corpus callosum.

between 2 and 4 mm. According to the cortical histological organisation, one distinguishes 6 layers numbered from I to VI from top to bottom [19]. In the spectral image, the cortex is separated in four different regions. One of the most pronounced difference separating those regions is the composition in myelin. Indeed, layer VI, adjacent to the CC clearly identified in the spectral map (cyan) is principally composed on elongated neuronal myelinated fibers that lie parallel to the CC neurons. This layer appeared particularly rich in myelin sheath. A second region (brown) is correlated with the layer V or pyramidal layer. This internal layer primarily contains pyramidal neurons whose apical dendrites are projected either in the molecular layer (layer I) or in the internal granular layer (layer IV). A third region corresponds to the layer II, III and IV in which myelinated fibers are less prominent. Finally the last region (yellow), corresponding to the molecular external layer (layer I) consisting of glial cells and nervous fibers with ways parallel to the cortical surface.

During tumor development, tissue composition and concentration of lipids decreased. This loss of lipids, correlated with demyelination, observed in different disorders, could be used as a spectroscopic marker. These results are in agreement with those obtained in brain pathologies [20], whereas, observations in other tumor types revealed an increase of lipids in tumor tissue [21]. Kraft *et al*. have investigated the lipid content of the white matter of human brain tissue using near infrared Raman spectroscopy [22]. They reported that the brain lipids can be divided into three principal classes: neutral lipids, phospholipids and sphingolipids. Increased levels of cholesterol esters (particularly cholesterol oleate and cholesterol linoleate) in glioma tissue have been reported before [23–25]. In these studies and in ours, necrotic and vital tumor

regions were not separately investigated, and therefore, no specific information regarding the biochemical composition of these distinct tumor regions was obtained. Previous studies on brain tumors using proton magnetic resonance spectroscopy [26–28,] also provided evidence of mobile lipid resonances (resonances arising from fatty acyl chains of lipids), possibly caused by cell proliferation arrest and necrosis. These findings were confirmed by other magnetic resonance spectroscopy studies in which the morphologic and biochemical features were compared [29–31].

We were also interested to surrounding tumor tissue. Indeed, in our FT-IRM data, we have detected one different structure (component 9) around the tumor. This structure could be attributed to the peritumoral oedema observed during glioma development. In fact, brain tumors contain new vessels that may have different structural properties favouring the formation of oedema within and around the tumor [18]. This oedema associated with brain tumor is due to an increase in the permeability of the blood–brain barrier and aggravate the mass effect of tumors. The diagnosis of peritumoral brain oedema is assisted by the use of imaging techniques such as computed tomography, magnetic resonance imaging, and spectroscopy. As tumors enlarge, they produce angiogenic factors that promote the emergence of new capillaries to supply the growing tumors. Newly formed capillaries are fenestrated and present less tight junctions, leading to the development of a peritumoral oedema. Moreover, C6 glioma cells in culture demonstrated secretion of diffusible factor that increase capillary permeability [32]. On the other hand, the surrounding tumor tissue is associated to the infiltrative zone. Indeed, glioblastoma typically grow through the surrounding brain parenchyma, intermingling with normal and reactive cells. Ide et al. found a correlation between peritumoral brain oedema and brain parenchyma destruction by the tumor [18]. In fact, this alteration corresponds to the myelin degradation in order to allow the infiltration of tumor cells. Myelin is responsible for the inhibition of cellular migration, and thus, the invasive process requires degradation of different myelin components [33]. Invasion is partially due to proteases that penetrate the surrounding tissue, induce vascular remodelling and destroy extracellular matrix [34].

This study demonstrates the potential of FT-IRM in successfully discriminating between normal brain structures, tumoral, and surrounding tumoral tissues. The structural changes were mainly related to qualitative and quantitative changes of lipids and will be used as spectroscopic markers for this pathology. In our FT-IRM data, the structure detected around the tumor could be attributed to the peritumoral oedema observed during glioma development. FT-IRM, with high spatially resolved morphological and biochemical information could be used as a diagnostic tool, complementary to histopathology to understand the molecular changes associated with tissue alteration. Future work will allow the quantification of biochemical changes (lipid and proteins) between healthy and tumor tissues by fitting the measured spectra with linear combination of the spectra of major pure components.

Acknowledgements

N. Amharref acknowledges financial support from the Conseil Régional Champagne-Ardenne. The authors are thankful to Ligue Marne, France, for financial support. The authors would also like to thank Pr. M. Kaltenbach for providing assistance in the preparation of the manuscript.

References

[1] P. Kleihues, L.H. Sobin, World Health Organization classification of tumors, Cancer 88 (2000) 2887.
[2] L.A. Stewart, Chemotherapy in adult high-grade glioma: a systematic review and meta-analysis of individual patient data from 12 randomised trials, Lancet 359 (2002) 1011–1018.
[3] M. Jackson, H.H. Mantsch, Biomedical Applications of Spectroscopy, Wiley, New York, 1996.
[4] P. Lasch, D. Naumann, FT-IR microspectroscopic imaging of human carcinoma thin sections based on pattern recognition techniques, Cell. Mol. Biol. 44 (1998) 189–202.
[5] A.T. Belien, P.A. Paganetti, M.E. Schwab, Membrane-type 1 matrix metalloprotease (MT1-MMP) enables invasive migration of glioma cells in central nervous system white matter, J. Cell. Biol. 144 (1999) 373–384.
[6] F. Gasparri, M. Muzio, Monitoring of apoptosis of HL60 cells by Fourier-transform infrared spectroscopy, Biochem. J. 369 (2003) 239–248.
[7] N. Gault, J.L. Lefaix, Infrared microspectroscopic characteristics of radiation-induced apoptosis in human lymphocytes, Radiat. Res. 160 (2003) 238–250.
[8] A. Gaigneaux, J.M. Ruysschaert, E. Goormaghtigh, Infrared spectroscopy as a tool for discrimination between sensitive and multiresistant K562 cells, Eur. J. Biochem. 269 (2002) 1968–1973.
[9] J. Ramesh, M. Huleihel, J. Mordehai, A. Moser, V. Erukhimovich, C. Levi, J. Kapelushnik, S. Mordechai, Preliminary results of evaluation of progress in chemotherapy for childhood leukemia patients employing Fourier-transform infrared microspectroscopy and cluster analysis, J. Lab. Clin. Med. 141 (2003) 385–394.
[10] P. Benda, J. Lightbody, G. Sato, L. Levine, W. Sweet, Differentiated rat glial cell strain in tissue culture, Science 161 (1968) 370–371.
[11] R.J. Barnes, M.S. Dhanoa, S.J. Lister, Standard normal variate transformation and detrending of near-infrared diffuse reflectance spectra, Appl. Spectrosc. 43 (1989) 772–777.
[12] J.B. McQueen, Some methods of classification and analysis of multivariate observations, in: L.M. LeCam, J. Neymann (Eds.), Proceedings of Fifth Berkeley Symposium on Mathematical Statistics and Probability, University of California, Berkeley, 1967, pp. 281–297.
[13] D.L. Massart, L. Kaufmann, The Interpretation of Analytical Chemical Data by the Use of Cluster Analysis, Wiley, New York, 1983.
[14] R.K. Dukor, M.N. Liebman, B.L. Johnson, A new, non-destructive method for analysis of clinical samples with FT-IR microspectroscopy. Breast cancer tissue as an example, Cell. Mol. Biol. 44 (1998) 211–217.
[15] F.S. Parker, Application of Infrared Spectroscopy in Biochemistry, Biology and Medicine, Plenum, New York, 1971.
[16] T. Yamada, N. Miyoshi, T. Ogawa, K. Akao, M. Fukuda, T. Ogasawara, Y. Kitagawa, K. Sano, Observation of molecular changes of a necrotic tissue from a murine carcinoma by Fourier-transform infrared microspectroscopy, Clin. Cancer Res. 8 (2002) 2010–2014.
[17] J. deGroot, Correlative Neuroanatomy, Appleton and Lange, Norwalk, 1991.
[18] M. Ide, M. Jimbo, O. Kubo, M. Yamamoto, H. Imanaga, Peritumoral brain edema associated with meningioma-histological study of the tumor margin and surrounding brain, Neurol. Med.-Chir. 32 (1992) 65–71.
[19] R.D. Burwell, Borders and cytoarchitecture of the perirhinal and postrhinal cortices in the rat, J. Comp. Neurol. 437 (2001) 17–41.
[20] J. Kneipp, P. Lasch, E. Baldauf, M. Beekes, D. Naumann, Detection of pathological molecular alterations in scrapie-infected hamster brain by Fourier transform infrared spectroscopy, Biochim. Biophys. Acta 1501 (2000) 189–199.

[21] L. Chiriboga, P. Xie, H. Yee, D. Zarou, D. Zakim, M. Diem, Infrared spectroscopy of human tissue. IV. Detection of dysplastic and neoplastic changes of human cervical tissue via infrared microscopy, Cell. Mol. Biol. 44 (1998) 219–229.
[22] C. Krafft, L. Neudert, T. Simat, R. Salzer, Near infrared Raman spectra of human brain lipids, Spectrochim. Acta, A: Mol. Biomol. Spectrosc. 61 (2005) 1529–1535.
[23] R. Campanella, Membrane lipids modifications in human gliomas of different degree of malignancy, J. Neurosurg. Sci. 36 (1992) 11–25.
[24] K. Gopel, E. Grassi, P. Paoletti, M. Usardi, Lipid composition of human intracranial tumors: a biochemical study, Acta. Neurochir. 11 (1963) 333.
[25] C. Nygren, H. von Holst, J-E. Månsson, P. Fredman, Increased levels of cholesterol esters in glioma tissue and surrounding areas of human brain, Br. J. Neurosurg. 11 (1997) 216–220.
[26] I. BarbaI, M.E. Cabañas, C. Arús, The relationship between nuclear magnetic resonance-visible lipids, lipid droplets, and cell proliferation in cultured C6 cells, Cancer. Res. 59 (1999) 1861–1868.
[27] W.G. Negendank, R. Sauter, T.R. Brown, J.L. Evelhoch, A. Falini, E.D. Gotsis, A. Heerschap, K. Kamada, B.C. Lee, M.M. Mengeot, E. Moser, K.A. Padavic-Shaller, J.A. Sanders, T.A. Spraggins, A.E. Stillman, B. Terwey, T.J. Vogl, K. Wicklow, R.A. Zimmerman, Proton magnetic resonance spectroscopy in patients with glial tumors: a multicenter study, J. Neurosurg. 84 (1996) 449–458.
[28] C. Rémy, N. Fouilhé, I. Barba, E. Sam-Laï, H. Lahrech, M.-G. Cucurella, M. Izquierdo, A. Moreno, A. Ziegler, R. Massarelli, M. Décorps, C. Arús, Evidence that mobile lipids detected in rat brain glioma by 1H nuclear magnetic resonance correspond to lipid droplets, Cancer Res. 57 (1997) 404–414.
[29] A.C. Kuesel, K.M. Briere, W. Halliday, G.R. Sutherland, S.M. Donnelly, I.C. Smith, Mobile lipid accumulation in necrotic tissue of high grade astrocytomas, Anticancer Res. 16 (1996) 1845–1849.
[30] A.C. Kuesel, S.M. Donnelly, W. Halliday, G.R. Sutherland, I.C. Smith, Mobile lipids and metabolic heterogeneity of brain tumors as detectable by ex vivo 1H MR spectroscopy, NMR Biomed. 7 (1994) 172–180.
[31] A.C. Kuesel, G.R. Sutherland, W. Halliday, I.C. Smith, 1H MRS of high grade astrocytomas: Mobile lipid accumulation in necrotic tissue, NMR Biomed. 7 (1994) 149–155.
[32] T. Ohnishi, P.B. Sher, J.B. Posner, W.R. Shapiro, Increased capillary permeability in rat brain induced by factors secreted by cultured C6 glioma cells: role in peritumoral brain edema, J. Neuro-oncol. 10 (1991) 13–25.
[33] A.A. Spillmann, V.R. Amberger, M.E. Schwab, High molecular weight protein of human central nervous system myelin inhibits neurite outgrowth: an effect which can be neutralized by the monoclonal antibody IN-1, Eur. J. Neurosci. 9 (1997) 549–555.
[34] B. Garbay, A.M. Heape, F. Sargueil, C. Cassagne, Myelin synthesis in the peripheral nervous system, Prog. neurobiol. 61 (2000) 267–304.